PAPER

Check for updates

Nano-assemblies of a soluble conjugated organic polymer and an inorganic semiconductor for sacrificial photocatalytic hydrogen production from water†

Haofan Yang,[a,b] Houari Amari,[c] Lunjie Liu,[a] Chengxi Zhao,[a] Hui Gao,[a] Ai He,[a] Nigel D. Browning,[c] Marc A. Little,[a] Reiner Sebastian Sprick [ID] *[a,d] and Andrew I. Cooper [ID] *[a,b]

Nanostructured materials have interesting optical and electronic properties that are often drastically different from those of their bulk counterparts. While bulk organic/inorganic semiconductor composites have attracted much attention in the past decade, the preparation of organic/inorganic semiconductor nanocomposites (OISNs) still remains challenging. This work presents an assembly method for the co-encapsulation of titanium dioxide dots (TDs) with a cyano-substituted soluble conjugated polymer (CSCP) into a particular nanoparticle. The as-prepared CSCP/TD semiconductor nanocomposites (CSCP/TD NCs) exhibit different particle surfaces and morphologies depending on the mass ratio of the CSCP to TDs. We then tested them as photocatalysts for sacrificial hydrogen production from water. We found that nanocomposites outperformed nanoparticles of the individual components and physical mixtures thereof. The most active CSCP/TD NC had a catalytic H_2 production rate that was 4.25 times higher than that of pure polymer nanoparticles prepared under the same conditions. We ascribe this to energy transfer between the semiconductors, where direct phase contact is essential, highlighting a potential avenue for using soluble, visible light-absorbing conjugated organic polymers to build Z-schemes for overall water splitting in the future.

Introduction

Multifunctional nano-objects containing discrete domains of different inorganic materials are of interest because they can demonstrate optical, magnetic, or electronic properties that are superior to those of the individual constituent materials.[1] Such nanocomposites are often formed through the seeded growth of one material on seed particles of another, thus yielding inorganic nanocomposites with core–shell or dumbbell-like morphologies.[2–7] Other preparation methods include physical mixing of different nanoparticles and embedding

multiple inorganic nanoparticles within a silica matrix.[8–10] Recently, the assembly of multiple building blocks into clusters using the so-called evaporation induced self-assembly (EISA) method has been reported.[11] This approach allows for quantum dots (QDs) to be assembled into large nanoparticle superstructures, *e.g.*, CdSe/TiO₂ colloidal spheres[12] and CdSe/ multishell supraparticles.[13] The CdSe/Au nanocomposites prepared *via* EISA exhibited higher photocatalytic activity for hydrogen production from water and better stability compared to the CdSe nanocrystal clusters alone.[14]

This approach has been shown to be transferable to organic/inorganic nanocomposites and was used to prepare a nanocomposite containing inorganic QDs and solution-processable alkyl polymers.[1,11,15–17] To do this, nano-sized hydrophobic droplets containing the solution-processable polymer and the inorganic QDs were well dispersed in water with the aid of a surfactant. By desolvating the hydrophobic droplets, the inorganic QDs were incorporated into the polymer nanoparticle matrix. Such organic/inorganic nanocomposites offer promise for application in nanomedicine through the combination of diagnostic and therapeutic components in a single delivery system.[1,18,19] None of the reported polymers showed

[a]*Department of Chemistry and Materials Innovation Factory, University of Liverpool, 51 Oxford Street, Liverpool L7 3NY, UK. E-mail: aicooper@liverpool.ac.uk*
[b]*Leverhulme Research Centre for Functional Materials Design, University of Liverpool, Liverpool L69 7ZD, UK*
[c]*Department of Mechanical, Materials & Aerospace Engineering, University of Liverpool, Liverpool L69 3GH, UK*
[d]*Department of Pure and Applied Chemistry, University of Strathclyde, Thomas Graham Building, 295 Cathedral Street, Glasgow G1 1XL, UK.*
E-mail: sebastian.sprick@strath.ac.uk
†Electronic supplementary information (ESI) available. See DOI: 10.1039/d0nr05801g

extended conjugation, and we saw potential to extend this approach into other areas, specifically for photocatalysis.

Composites of inorganic photocatalysts with organic photocatalysts have been extensively studied; in particular, carbon nitrides have shown excellent performance as photocatalysts for hydrogen production from water in the presence of a sacrificial hole scavenger.[20–22] However, these composites cannot be obtained using solution-based methods because the constituent components are not soluble, which limits the range of synthetic tuneability. Conjugated polymer nanocomposites have been far less explored so far, but recent reports of composites of pyrene-based conjugated microporous polymers (CMPs) with MoS_2[23] and tri/diethynylbenzene-benzothiadiazole polymers with TiO_2[24,25] have shown promise. However, an *in situ* polymerization approach was used in both of these studies, where the inorganic component was added to the monomers before performing the polymerization. This introduces synthetic limitations and, more importantly, reduces control over the physical incorporation of the inorganic components. Since most conjugated polymer photocatalysts reported to date are not solution processable,[26,27] solution-based methods such as EISA cannot be used widely to prepare composites. However, recent reports of soluble conjugated polymer photocatalysts[28,29] have now made it possible to synthesize organic/inorganic semiconductor nanocomposites using EISA.

Here we use photocatalytically active TiO_2[30–32] and a soluble conjugated polymer (CSCP) to form $CSCP/TiO_2$ nanocomposites (NCs) using an oil-in-water emulsion solvent evaporation method. The morphology of the resulting nanoparticles changed with increasing content of the TiO_2 dots (TDs), and we studied the energy transfer between the components using UV-vis and photoluminescence spectroscopy. Finally, we tested these nanocomposites for sacrificial photocatalytic hydrogen production from water and observed a clear trend within the series, with a maximum catalytic efficiency at a CSCP-to-TD ratio of 10 : 90 w/w%. Control studies confirmed that the formation of a nanocomposite interface is required for this increased photocatalytic activity, and the effect was not seen with physical mixtures that were not produced *via* the EISA route.

Results and discussion

First, titanium dioxide dots (TDs) were prepared using a modified wet-chemical procedure with oleylamine (*cis*-1-amino-9-octadecene) and oleic acid ((9Z)-octadec-9-enoic acid) as the surfactants (ESI†).[33] The surfactants solubilise the TDs in chloroform and serve as stabilizing ligands.[14,34] High resolution transmission electron microscopy (HR-TEM) imaging showed uniform TDs of approximately 2.7 nm diameter (Fig. S1†). Powder X-ray diffraction (PXRD) analysis showed that the TDs were obtained solely as TiO_2 in the anatase phase (Fig. S2†). The soluble organic polymer photocatalyst [poly(di-n-octyl-9H-fluorene-co-cyanobenzene), CSCP] was synthesized *via* the Pd(0)-catalyzed Suzuki–Miyaura polycondensation of

dibromobenzonitrile and the diboronic acid ester of di-n-octyl-9H-fluorene in toluene at 80 °C (Fig. S3†).[28,35] After work-up and Soxhlet extraction, the polymer was found to be also soluble in chloroform, which allowed for solution characterization and solution processing. Fourier-transform infrared spectroscopy (FT-IR) showed the presence of the expected alkyl C–H functionalities in polymer side chains (3000–2800 cm^{-1}), and a characteristic band for the cyano group at approximately 2225 cm^{-1} (Fig. S4†). The structure was also confirmed by solution ^{1}H NMR spectroscopy (Fig. S5†) and the weight average molecular weight of the polymer was estimated to be 22.3 kg mol^{-1} by gel permeation chromatography, as calibrated against polystyrene standards (Fig. S6†). Residual palladium was found in the polymer sample at a concentration of 0.35 wt%, as measured by inductively coupled plasma mass spectrometry; this originates from the palladium catalyst used for the polycondensation reaction.

Both the TDs and the CSCP were soluble in chloroform and this allowed them to be combined in an oil-in-water emulsion process, which was used to prepare hybrid assemblies. To do this, the CSCP was dissolved in chloroform along with the TDs, and this solution was emulsified in water containing the sodium n-dodecyl sulfate (SDS) surfactant using an ultrasonic probe to produce a uniform emulsion. The emulsion solution was then stirred at 40 °C for around 14 hours to remove chloroform by evaporation to afford the co-assembled CSCP/TD NCs as a clear solution, denoted hereafter as NCX%, where X is the weight percentage of the polymer in the composite. The same conditions were also used to obtain nanoparticles (NPs) of the individual components, that is, CSCP-assembled nanoparticles (CSCP NPs) and TD-assembled nanoparticles (TD NPs), as shown in Fig. 1. We note that turbid solutions were generally obtained without stirring, indicating the formation of (undesirable) larger aggregates. After purification by dialysis for 3 days, nanocomposites containing more than 75 w/w% of TDs seemed to undergo aggregation and sedimentation was observed (Fig. S8 and S9†).

As a result of chloroform evaporation when preparing the nanocomposites, the increase in solvent polarity forces solvophobic association between stabilizing ligands, which is often observed in the 1D self-assembly of surfactants and other amphiphilic molecules (Fig. S7†).[34,36,37] Various imaging techniques were used to study the morphology of the materials: the scanning electron microscopy (SEM) images in high magnification showed that the materials were uniform spheres and statistical analysis showed that similar average sizes for TD NPs, CSCP NPs and CSCP/TD NCs were obtained (Fig. 2a and Fig. S10†). For TD nanoparticles without the CSCP, scanning transmission electron microscopy (STEM) images showed that multiple TDs were stacked together to form each nanoparticle (Fig. 2b). The binding energy of Ti L edges was around 458 eV in TDs, as estimated by STEM-electron energy loss spectroscopy (STEM-EELS, Fig. S11†). The fast Fourier transform (FTT) pattern of TD NPs (Fig. 2b) showed lattice fringes with d-spacing at 0.34, 0.23 and 0.18 nm, which can be ascribed to the (101), (004) and (200) planes of the anatase TiO_2 phase, in agreement with its PXRD pattern (Fig. S12†). The STEM
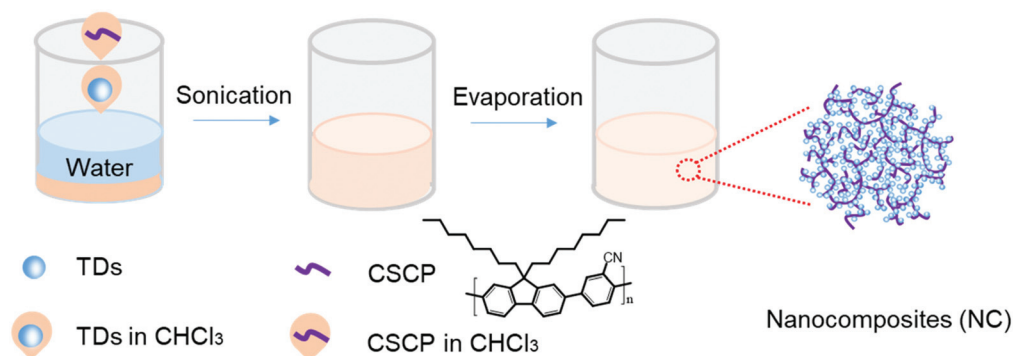
Fig. 1 Synthesis of the nanoparticles and nanocomposites: the soluble conjugated polymer (CSCP) and TiO$_2$ dots (TDs) are dissolved in chloroform (2 mL) and then emulsified with water (10 mL) in the presence of a surfactant (sodium *n*-dodecyl sulfate) by ultrasonication.
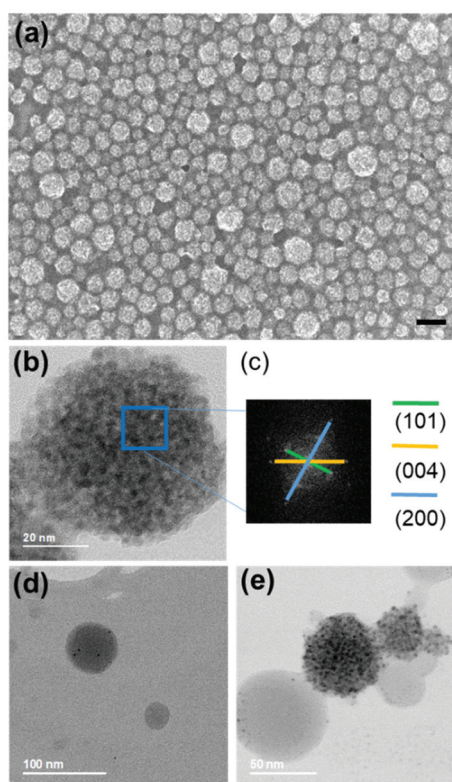

Fig. 2 Morphology and internal structures of the assembled TD and CSCP nanoparticles (nanocomposites are shown in Fig. 3). (a) High resolution FE-SEM images of TD NPs (scale bar is 100 nm long); (b) STEM images of TD NPs; (c) fast Fourier transform diffraction pattern of the highlighted area; (d) STEM image of CSCP NPs and (e) 50% CSCP + 50% TD NP physical mixture.

Next, we studied the internal structure of the CSCP/TD NCs using both bright field STEM and high-angle annular dark-field STEM (HAADF-STEM), which showed that the materials obtained from the emulsion process are not phase separated but are instead co-assembled nanocomposites of the polymer and TiO$_2$. In the case of samples consisting mostly of the polymer (NC90% under bright field STEM, Fig. 3a), the TDs were found to be uniformly distributed within the nanocomposite, with few TDs exposed on the nanoparticle surface, resulting in a smooth surface. With an increased loading of TDs (NC50%, Fig. 3c), the surface of the nanocomposite becomes rougher and more TDs are exposed on the surface.
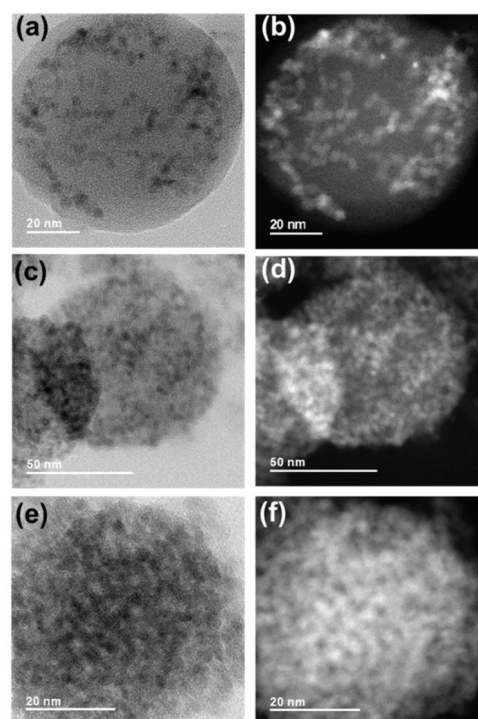

Fig. 3 Morphology and internal structures of nanocomposites. Bright field STEM images of (a) NC90%, (c) NC50% and (e) NC10%. HAADF-STEM images of (b) NC90%, (d) NC50% and (f) NC10%.

images of pure CSCP nanoparticles showed that these have a smooth surface and residual palladium was found to be present as nanoparticles (Fig. 2d). When both the CSCP and TD NPs were mixed together as a physical mixture, it was possible to identify both of the phases clearly by STEM, as evident from a physical mixture of the CSCP and TD NPs in a weight ratio of 1 : 1 (50% CSCP + 50% TDs, Fig. 2e).

For a highly loaded TD nanocomposite, NC10%, no clear domains of the polymer were visible, suggesting that the amorphous polymer is embedded between the inorganic TDs. HAADF-STEM imaging was also used to provide a clear contrast between the CSCP (dark in HADDF-STEM images) and TDs (bright in HADDF-STEM images) due to the large difference in their atomic numbers (Fig. 2b, d and f). Compared with NC10% (Fig. 3f), the HAADF-STEM image for NC50% (Fig. 3d) exhibits more dark areas in the nanoparticle domain, suggesting the embedding of a greater amount of the amorphous polymer.

The UV–Vis absorption spectra were obtained in an aqueous suspension for the samples before dialysis (Fig. 4). All materials were found to absorb light between 300 and 420 nm, with a characteristic peak of the CSCP centered around 364 nm for the as-prepared nanoparticles and nanocomposites. By contrast, TDs absorb light only below 350 nm, which is typical of TiO_2 and related materials.[38] Within the nanocomposite series, the absorption peak of the CSCP gradually decreases with decreasing amounts of the CSCP. Moreover, the peak maximum is shifted from 364 nm for 25% CSCP + 75% TDs to 370 nm for NC25%. The observed shift in the case of the nanocomposites suggests an interaction between the CSCP and the TDs and might also indicate that direct intimate contact is required for this interaction to occur between the two materials. Moreover, physical mixtures do not show a shift in the absorption, further showing the importance of intimate contact in the nanocomposites. From UV-Vis measurements, an optical gap (E_g^{op}) of 2.75 eV was determined for the CSCP (Fig. S13†), which is close to the predicted gap using density functional theory (Fig. 14, ESI†). The HOMO energy level of the CSCP was found to be 0.5 eV via cyclic voltammetry (Fig. S15, ESI†) and the LUMO energy level was calculated to be −2.25 eV. The conduction band of TDs is below the LUMO energy level of the polymer, but above its HOMO energy level at −0.2 eV, while the valence band of the TQDs is much lower at 3.2 eV.[33]

Steady-state photoluminescence was measured in an aqueous suspension with excitation at 360 nm (Fig. 5a). The CSCP NPs and nanocomposites showed strong emission peaks

Fig. 5 (a) Fluorescence intensity of TD NPs, CSCP NPs, TD + CSCP NP physical mixtures and CSCP/TD NCs under 360 nm excitation measured at room temperature; (b) TRSPC decays monitored at 480 nm under 370.5 nm excitation at room temperature; (c) photocatalytic hydrogen production rates under 1 sun irradiation for the NCs plotted as a function of the weight ratio of the CSCP to TDs (0/100 corresponds to the pure TD nanoparticles). Conditions: Catalyst 192.3 µg mL^{-1} (1 mg in 5.2 mL total volume), TEOA (10 vol% in water), 5 hours of irradiation with an ABA solar simulator; (d) time course of hydrogen production under broadband illumination of TD NPs, CSCP NPs, and NC10%. Conditions: Catalyst 2 mg in 20 mL of aqueous TEOA (10 vol%), 5 hours of irradiation with a 300 W Xe light source fitted with a λ > 295 nm filter.

at approximately 420 and 440 nm, while the TD NPs showed only a weak fluorescence emission due to the electron transition mediated by defects in the band gap.[39] The nanocomposite NC10% shows emission originating from the CSCP, which is at a much higher intensity when compared to the physical mixture (10% CSCP + 90% TD NPs), showing that intimate contact is required for energy transfer to occur. When the excitation is at 400 nm and beyond, that is beyond the absorption onset of the TDs, a drop in the intensity of the emission of the CSCP was observed (Fig. S16 and S17†), further supporting that energy transfer between the TDs and the CSCP takes place in the nanocomposites.

The average lifetimes of the excited state lifetimes were estimated by performing time-resolved single photon counting (TRSPC) experiments (Fig. 5b and Table S1†). The CSCP was found to have a short average photoluminescence (PL) lifetime (3.37 ns), which is typically observed for these kinds of conjugated polymers.[40,41] The TDs were found to have a weak emission, in line with the PL experiments, but a longer average PL lifetime (7.57 ns). The nanocomposites had shorter lifetimes – e.g., NC10% (4.35 ns) – compared to the TDs, but nevertheless longer lifetimes than that of the CSCP. When comparing physical mixtures of TD and CSCP NPs to nanocomposites, shorter lifetimes were observed. For example, the physical mixture of 10% CSCP + 90% TD NPs had a shorter lifetime (3.38 ns) compared to the nanocomposite of the same composition (NC10%, τ = 4.35 ns).
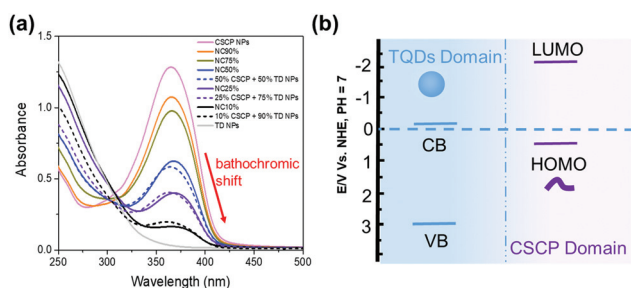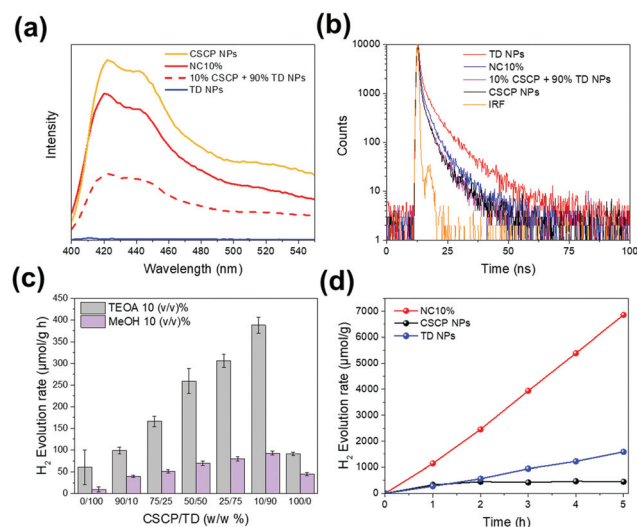
Fig. 4 (a) UV-Vis absorption spectra obtained in an aqueous suspension of TD NPs, CSCP NPs, TD + CSCP NP physical mixtures and CSCP/TD NCs with various compositions. All measurements were performed at the same concentration (16.7 mg L^{-1}). (b) Energy levels of the CSCP and TDs. LUMO: Lowest unoccupied molecular orbital; HOMO: highest occupied molecular orbital; CB: conduction band; VB: valence band.

Further addition of TDs to a nanoparticle physical mixture of 10% CSCP + 90% TDs did not result in changes of the lifetime of the CSCP, showing that no material interaction occurs in the absence of intimate phase contact. Taken together, this shows that the difference in the lifetime of the nanocomposites compared to those of the conjugated polymer and the TDs is not a simple additive effect but stems from energy transfer within the nanocomposites.

Compared to the physical mixtures of nanoparticles, the nanocomposites exhibit bathochromic shifted absorption, enhanced PL emission, and prolonged decay in the PL lifetime. These facts suggest the communication or energy transfer between TDs and CSCP, which might be expected to enhance the photocatalytic performance of the nanocomposites compared to those of the individual components. We tested the photocatalytic activity of the CSCP/TD nanocomposites for sacrificial hydrogen production from water using a high-throughput workflow that was described previously.[40,42] For these measurements, samples were added to vials, transferred to a liquid handling system, and inertized under nitrogen. Then, in the liquid handling system, water and the hole scavenger were added before the vials were capped. After this, the samples were transferred to a solar simulator and illuminated with constant agitation before measuring the hydrogen production using an automated gas chromatograph.

The materials and nanocomposites were tested as prepared without any additional metal; residual palladium from the synthesis (*vide supra*) acts as the co-catalyst.[35,43] We tested two different hole scavengers in this study, triethanolamine (TEOA), which is typically used for organic photocatalysts such as carbon nitrides,[44] and methanol, which is typically used for titanium dioxide.[45] Hydrogen evolution rates (HERs) were determined using 1 mg in 5.2 mL water/scavenger mixture and normalized to the total mass of both photocatalysts in the nanocomposite, their physical mixtures or the individual photocatalysts. All nanocomposites, as well as individual TD and CSCP NPs, produced hydrogen from water using methanol, but higher overall HERs were obtained when TEOA was used as the hole scavenger (Fig. 5c). The TD NPs produced hydrogen at a rate of 60.1 μmol g^{-1} h^{-1} when TEOA was used as the scavenger, which steadily increased with increasing content of the inorganic photocatalyst TD in the composite up to 90 w/w%. The nanocomposite NC10% had the highest HER of all composites with a rate of 387.8 μmol g^{-1} h^{-1}. By comparison, nanoparticles of the polymer, CSCP, have a rate of only 90.7 μmol g^{-1} h^{-1} under the same conditions.

Physical mixtures of the CSCP and TD NPs, obtained by mixing both materials immediately before the photocatalysis experiment, gave significantly lower hydrogen evolution rates of 83.2 μmol g^{-1} h^{-1} and 69.7 μmol g^{-1} h^{-1} for 50% CSCP + 50% TD and 10% CSCP + 90% TD NPs (Fig. S18†), respectively, compared to their analogous nanocomposites, which showed hydrogen evolution rates of 259.3 μmol g^{-1} h^{-1} for NC50% and 387.8 μmol g^{-1} h^{-1} for NC10%. This shows that the production of inorganic–organic nanocomposites enhances the photo-

catalytic activity significantly and also suggests that the phase contact between the TDs and the CSCP plays a key role. The kinetic hydrogen evolution experiment measurements under broadband irradiation ($\lambda > 295$ nm, 300 W Xe light source) under otherwise identical conditions showed that NC10% afforded a higher HER of 1371.2 μmol g^{-1} h^{-1} (Fig. 5d), with no obvious reduction in activity observed during 18 hours of illumination (Fig. S19†), suggesting good stability of the nanocomposite photocatalysts. NC10% also afforded a HER of 148.7 μmol g^{-1} h^{-1} under visible light irradiation ($\lambda > 395$ nm, 300 W Xe light source) (Fig. S20†). After photocatalysis, no obvious changes in the UV-Vis absorption spectrum and particle morphology of NC10% compared to the as-prepared sample were found (Fig. S21 and S22†). Control experiments showed that no hydrogen production occurred in the absence of a photocatalyst. Nanoparticles of the CSCP and the TDs also showed no appreciable hydrogen production in the dark or under illumination without a hole scavenger.

The CSCP/TD nanocomposites were found to produce trace amounts of hydrogen without a hole scavenger (Fig. S23†). To rule out that hydrogen originates from the decomposition of the organic polymer by the TD nanoparticles, we prepared a nanocomposite with a non-conjugated polymer, namely polystyrene. This nanocomposite of photo-inactive polystyrene and TDs (Fig. S24†) showed similar particle shapes and size distributions to those of the analogous CSCP/TD NCs as evident from SEM imaging (Fig. S10†), but it did not produce any hydrogen in the absence of a scavenger under illumination, suggesting that the generation of H$_2$ in the nanocomposites may not originate from polymer decomposition. Also, significantly lower amounts of hydrogen were produced in the presence of TEOA for the polystyrene/TD nanocomposite (47.2 μmol g^{-1} h^{-1}) compared to NC10% (387.8 μmol g^{-1} h^{-1}), suggesting that the photoactive CSCP contributed significantly to the enhanced HER of CSCP/TD NCs (Fig. S25†). We suspected that oleylamine, which was used as the stabilization ligand when preparing the nanocomposites, could be oxidised and act as the hole scavenger as it contains an amino group.[46] This was confirmed by adding oleylamine to the CSCP nanoparticles in water containing 10% of methanol, which resulted in the production of a higher amount of hydrogen (284.4 μmol g^{-1} h^{-1} for an additional 0.05 mL of oleylamine) compared to experiments with only methanol as the scavenger (51.4 μmol g^{-1} h^{-1}; Fig. S26†). The apparent quantum yields (AQYs) for NC10% were determined to be 0.05% at 420 nm, 0.34% at 395 nm and 1.08% at 340 nm, broadly following the absorption spectrum of the composite further suggesting that the hydrogen generation is a photocatalytic process (Fig. S27 of the ESI†).

In a previous work, a degree of aggregation of polymer nanoparticles was shown to improve the photocatalytic performance, possibly because of increased light scattering of these highly translucent suspensions.[47] This was also explored as a possibility here by preparing aggregates of the bulk CSCP and CSCP nanoparticles with photocatalytically inactive SiO$_2$ nanoparticles to give composites that contained 10% polymer and 90% SiO$_2$. The bulk CSCP polymer/SiO$_2$ composites did

not produce hydrogen, and the polymer nanoparticles/SiO_2 composites produced hydrogen at a very low rate of 40.2 μmol g^{-1} h^{-1} (Fig. S28†). This suggests that aggregation of the polymer particles was not the main factor in the enhanced photocatalytic activity of these nanocomposites, but it does not rule out that light scattering effects play a role here, too.

Conclusions

In conclusion, a range of nanocomposites comprising various ratios of an inorganic semiconductor and an organic polymer photocatalyst were prepared from nanoparticles using an emulsion-induced self-assembly method. The morphology of the nanocomposites was a function of the amount of TiO_2 loaded into the nanoparticles. These composites showed evidence of energy transfer between TD and CSCP NPs, resulting in changes in light absorption, PL emission, and emission decay behaviors. The nanocomposites showed enhanced sacrificial catalytic H_2 production from water compared with the nanoparticle counterparts produced from either the CSCP or the TDs. The composite containing NC10% was found to have the highest activity, outperforming the polymer alone by a factor of 4.3 and the TDs by a factor of 6.4. The advantage of this approach is that the conjugated polymer and QDs can be synthesized separately and then combined in a common organic solvent, allowing for the tuning of the polymer composition and thus allowing systematic control over the physical and chemical properties. The simplicity and versatility of this EISA method make it a powerful route for the preparation of many new multifunctional organic/inorganic semiconductor nanocomposites. In particular, it is a potential avenue for the preparation of organic–inorganic hybrid Z-scheme photocatalysts that do not rely on sacrificial reagents. For example, it should be possible to prepare heterostructures of hydrogen-evolving conjugated polymers with oxygen-evolving inorganic semiconductor catalysts.

Conflicts of interest

There are no conflicts to declare.

Acknowledgements

Notes and references

1 J. Bae, J. Lawrence, C. Miesch, A. Ribbe, W. Li, T. Emrick, J. Zhu and R. C. Hayward, *Adv. Mater.*, 2012, **24**, 2735–2741.

2 F. Wang, R. Deng, J. Wang, Q. Wang, Y. Han, H. Zhu, X. Chen and X. Liu, *Nat. Mater.*, 2011, **10**, 968–973.

3 W. Shi, H. Zeng, Y. Sahoo, T. Y. Ohulchanskyy, Y. Ding, Z. L. Wang, M. Swihart and P. N. Prasad, *Nano Lett.*, 2006, **6**, 875–881.

4 H. Gu, R. Zheng, X. X. Zhang and B. Xu, *J. Am. Chem. Soc.*, 2004, **126**, 5664–5665.

5 H. Yu, M. Chen, P. M. Rice, S. X. Wang, R. L. White and S. Sun, *Nano Lett.*, 2005, **5**, 379–382.

6 E. V. Shevchenko, M. I. Bodnarchuk, M. V. Kovalenko, D. V. Talapin, R. K. Smith, S. Aloni, W. Heiss and A. P. Alivisatos, *Adv. Mater.*, 2008, **20**, 4323–4329.

7 H. Wen, H. Zhu, X. Chen, T. F. Hung, B. Wang, G. Zhu, S. F. Yu and F. Wang, *Angew. Chem., Int. Ed.*, 2013, **52**, 13419–13423.

8 A. Sousa-Castillo, M. Comesaña-Hermo, B. Rodríguez-González, M. Pérez-Lorenzo, Z. Wang, X. T. Kong, A. O. Govorov and M. A. Correa-Duarte, *J. Phys. Chem. C*, 2016, **120**, 11690–11699.

9 N. Insin, J. B. Tracy, H. Lee, J. P. Zimmer, R. M. Westervelt and M. G. Bawendi, *ACS Nano*, 2008, **2**, 197–202.

10 D. K. Yi, S. T. Selvan, S. S. Lee, G. C. Papaefthymiou, D. Kundaliya and J. Y. Ying, *J. Am. Chem. Soc.*, 2005, **127**, 4990–4991.

11 C. J. Brinker, Y. Lu, A. Sellinger and H. Fan, *Adv. Mater.*, 1999, **11**, 579–585.

12 L. Liu, J. Hensel, R. C. Fitzmorris, Y. Li and J. Z. Zhang, *J. Phys. Chem. Lett.*, 2010, **1**, 155–160.

13 D. Vanmaekelbergh, L. K. Van Vugt, H. E. Bakker, F. T. Rabouw, B. De Nijs, R. J. A. Van Dijk-Moes, M. A. Van Huis, P. J. Baesjou and A. Van Blaaderen, *ACS Nano*, 2015, **9**, 3942–3950.

14 R. Shi, Y. Cao, Y. Bao, Y. Zhao, G. I. N. Waterhouse, Z. Fang, L. Z. Wu, C. H. Tung, Y. Yin and T. Zhang, *Adv. Mater.*, 2017, **29**, 1–7.

15 T. Isojima, S. K. Suh, J. B. V. Sande and T. A. Hatton, *Langmuir*, 2009, **25**, 8292–8298.

16 J. H. Park, G. Von Maltzahn, E. Ruoslahti, S. N. Bhatia and M. J. Sailor, *Angew. Chem., Int. Ed.*, 2008, **47**, 7284–7288.

17 J. Shao, H. Xie, H. Huang, Z. Li, Z. Sun, Y. Xu, Q. Xiao, X. F. Yu, Y. Zhao, H. Zhang, H. Wang and P. K. Chu, *Nat. Commun.*, 2016, **7**, 1–13.

18 Z. Gu, A. Biswas, M. Zhao and Y. Tang, *Chem. Soc. Rev.*, 2011, **40**, 3638–3655.

19 J. Shi, A. R. Votruba, O. C. Farokhzad and R. Langer, *Nano Lett.*, 2010, **10**, 3223–3230.

20 Z. Zhao, Y. Sun and F. Dong, *Nanoscale*, 2015, **7**, 15–37.

21 G. Liao, Y. Gong, L. Zhang, H. Gao, G.-J. Yang and B. Fang, *Energy Environ. Sci.*, 2019, **12**, 2080–2147.

22 Y. Shi, J. Chen, Z. Mao, B. D. Fahlman and D. Wang, *J. Catal.*, 2017, **356**, 22–31.

23 S. Zang, G. Zhang, Z.-A. Lan, D. Zheng and X. Wang, *Appl. Catal., B*, 2019, **251**, 102–111.

24 Y. Xiang, X. Wang, X. Zhang, H. Hou, K. Dai, Q. Huang and H. Chen, *J. Mater. Chem. A*, 2018, **6**, 153–159.

25 X. Zhang, J. Xiao, M. Hou, Y. Xiang and H. Chen, *Appl. Catal., B*, 2018, **224**, 871–876.

26 Y. Wang, A. Vogel, M. Sachs, R. S. Sprick, L. Wilbraham, S. J. A. Moniz, R. Godin, M. A. Zwijnenburg, J. R. Durrant, A. I. Cooper and J. Tang, *Nat. Energy*, 2019, **4**, 746–760.

27 X. Wang, G. Zhang and Z.-A. Lan, *Angew. Chem., Int. Ed.*, 2016, **55**, 15712–15727.

28 D. J. Woods, R. S. Sprick, C. L. Smith, A. J. Cowan and A. I. Cooper, *Adv. Energy Mater.*, 2017, **7**, 1700479.

29 J. Kosco, M. Bidwell, H. Cha, T. Martin, C. T. Howells, M. Sachs, D. H. Anjum, S. Gonzalez Lopez, L. Zou, A. Wadsworth, W. Zhang, L. Zhang, J. Tellam, R. Sougrat, F. Laquai, D. M. DeLongchamp, J. R. Durrant and I. McCulloch, *Nat. Mater.*, 2020, **19**, 559–565.

30 Y. Wei, J. Wang, R. Yu, J. Wan and D. Wang, *Angew. Chem.*, 2019, **58**, 1422–1426.

31 X. Zhou, V. Häublein, N. Liu, N. T. Nguyen, E. M. Zolnhofer, H. Tsuchiya, M. S. Killian, K. Meyer, L. Frey and P. Schmuki, *Angew. Chem., Int. Ed.*, 2016, **55**, 3763–3767.

32 K. Fujishima and A. Honda, *Nature*, 1972, **238**, 37–38.

33 X. Xu, Z. Gao, Z. Cui, Y. Liang, Z. Li, S. Zhu, X. Yang and J. Ma, *ACS Appl. Mater. Interfaces*, 2016, **8**, 91–101.

34 Z. Huang, Y. Liu, Q. Zhang, X. Chang, A. Li, L. Deng, C. Yi, Y. Yang, N. M. Khashab, J. Gong and Z. Nie, *Nat. Commun.*, 2016, **7**, 1–8.

35 Y. Bai, D. J. Woods, L. Wilbraham, C. M. Aitchison, M. Zwijnenburg, R. S. Sprick and A. Cooper, *J. Mater. Chem. A*, 2020, **8**, 8700–8705.

36 S. E. Paramonov, H. W. Jun and J. D. Hartgerink, *J. Am. Chem. Soc.*, 2006, **128**, 7291–7298.

37 Y. Che, A. Datar, K. Balakrishnan and L. Zang, *J. Am. Chem. Soc.*, 2007, **129**, 7234–7235.

38 T. Baran, S. Wojtyła, A. Minguzzi, S. Rondinini and A. Vertova, *Appl. Catal., B*, 2019, **244**, 303–312.

39 Y. Zhao, C. Li, X. Liu, F. Gu, H. Jiang, W. Shao, L. Zhang and Y. He, *Mater. Lett.*, 2007, **61**, 79–83.

40 Y. Bai, L. Wilbraham, B. J. Slater, M. A. Zwijnenburg, R. S. Sprick and A. I. Cooper, *J. Am. Chem. Soc.*, 2019, **141**, 9063–9071.

41 M. Sachs, R. S. Sprick, D. Pearce, S. A. J. Hillman, A. Monti, A. A. Y. Guilbert, N. J. Brownbill, S. Dimitrov, X. Shi, F. Blanc, M. A. Zwijnenburg, J. Nelson, J. R. Durrant and A. I. Cooper, *Nat. Commun.*, 2018, **9**, 4968.

42 C. B. Meier, R. Clowes, E. Berardo, K. E. Jelfs, M. A. Zwijnenburg, R. S. Sprick and A. I. Cooper, *Chem. Mater.*, 2019, **31**, 8830–8838.

43 J. Kosco, M. Sachs, R. Godin, M. Kirkus, L. Francas, M. Bidwell, M. Qureshi, D. Anjum, J. R. Durrant and I. McCulloch, *Adv. Energy Mater.*, 2018, **8**, 1802181.

44 X. Wang, K. Maeda, A. Thomas, K. Takanabe, G. Xin, J. M. Carlsson, K. Domen and M. Antonietti, *Nat. Mater.*, 2009, **8**, 76–80.

45 Y. K. Kho, A. Iwase, W. Y. Teoh, L. Mädler, A. Kudo and R. Amal, *J. Phys. Chem. C*, 2010, **114**, 2821–2829.

46 Y. Pellegrin and F. Odobel, *C. R. Chim.*, 2017, **20**, 283–295.

47 C. M. Aitchison, R. S. Sprick and A. I. Cooper, *J. Mater. Chem. A*, 2019, **7**, 2490–2496.